J. Phys. IV France **11** (2001)

Lattice deformations at martensite-martensite interfaces in Ni-Al

D. Schryvers, Ph. Boullay*, R. Kohn[1] and J. Ball[2]

EMAT, University of Antwerp, RUCA, Groenenborgerlaan 171, 2020 Antwerpen, Belgium
[1] *Courant Institute of Mathematical Sciences, New York University, 251 Mercer Street, New York, NY 10012, U.S.A.*
[2] *Mathematical Institute, University of Oxford, St-Giles 24-29, Oxford OX1 3LB, U.K.*

Abstract: The atomic configurations at macrotwin interfaces between microtwinned martensite plates in $Ni_{65}Al_{35}$ material are investigated using high resolution transmission electron microscopy (HRTEM). The observed structures are interpreted in view of possible formation mechanisms of these interfaces. A distinction is made between cases in which the microtwins, originating from mutually perpendicular {110} austenite planes, enclose a final angle larger or smaller than 90°, measured over the boundary. Two different configurations, one with crossing microtwins and the other with ending microtwins producing a step configuration are described. The latter is related with the existence of microtwin sequences with changing variant widths. Although both features appear irrespective of the material's preparation technique, rapid solidification seems to prefer the step configuration. Depending on the actual case, tapering, bending and tip splitting of the small microtwin variants is observed. Severe lattice deformations and reorientations occur in a region of 5 – 10 nm around the interface while sequences of single plane ledges gradually bending the microtwins are found up to 50 nm away from the interface. These structures and deformations are interpreted in view of the need to accommodate any remaining stresses.

1. INTRODUCTION

The cubic-to-tetragonal thermoelastic martensitic transformation in Ni_xAl_{100-x} ($62 \leq x \leq 69$) results in the formation of multiply twinned martensite plates accommodating the shape change and minimising the elastic energy. Each plate consists of two of the three possible deformation variants U_1, U_2 and U_3 described by the diagonal matrix (η_1, η_1, η_3) and permutations hereof, where $\eta_1 < 1 < \eta_3$. The microtwin planes inside these martensite plates are close packed {111} type planes in the $L1_0$ description of the martensite structure and they originate from former {110} type planes of the B2 austenite. Within the concept of minimisation of the elastic energy the numerical values of the deformation parameters dictate the final volume fractions, rigid body rotations, habit plane normals, etc. Such plates can grow from different nucleation sites in the parent matrix and will form habit planes close to {101} type planes (i.e., families at 120° with respect to the {110} planes leading to the microtwins). When the transformation proceeds, each plate will continue to grow and finally martensite-martensite interfaces will be formed. When disregarding local differences in microtwin sequence, such interfaces can be referred to as macrotwin planes. Although interfaces between different martensite plates resulting from this type of transformation have been investigated before [1-4], no detailed study on the atomic configurations at these interfaces has been conducted so far for Ni-Al. It is clear that the local atomic structure of the interfaces could play an important role in the reversibility and thus the shape memory behaviour of these materials.

In the present paper an overview of different micro- and nanoscale configurations of such martensite-martensite interfaces will be presented. The formed interfaces will depend on the original choice of deformation variants, the actual orientation of the microtwin planes and the stability of the volume fractions on either side.

2. EXPERIMENTAL RESULTS

A typical example of a mesoscale view of an interface between two martensite plates in Ni-Al is shown in figure 1a. In this particular case, a number of different aspects of such interfaces are found. First it should be noted that, as the microtwins are observed edge-on in both plates and the involved planes originate from former {110) planes in the austenite, the macrotwin interface is on average parallel with former cubic planes of the parent phase, as seen from the schematic in figure 1b. As the actual orientations of the microtwin planes slightly deviate from the {110) cubic planes, the final angle α between these microtwins and measured over the interface also deviates from the original 90° in the austenite. As a direct result of the change in

* *Now at*: Laboratoire SPCTS, Faculté des Sciences, 123 avenue Albert Thomas, 87060 Limoges cedex, France.

orientation of the macrotwin at point A, this angle changes from larger to smaller than 90°. Typically deviations around 5° from the right angle are measured.

Second, two different structural features can be recognised in this image. Indeed, the macrotwin part close to parallel with a former (010) cubic plane primarily consists of crossing microtwins, i.e., the small variants of a given plate penetrate over approximately one large variant into the other plate. On the other hand, the macrotwin part close to parallel with a former (100) cubic plane is made up of a number of step-like configurations where a number of fine parallel microtwins of one plate stop at a broad variant of the other plate, locally resulting in an interface parallel with a {110) cubic plane. Alternating (110) with (1-10) planes yield the average (100) plane for this part of the interface. Although in the present example the crossings occur at the interface where $\alpha < 90°$ whereas the steps correspond with the $\alpha > 90°$ case, the alternative possibilities have also been observed so no direct correlation between these different aspects should be assumed [5].

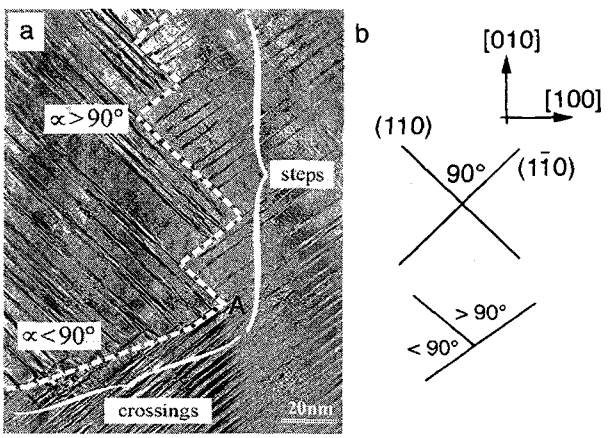

Figure 1: (a) Mesoscale view of an interface between two martensite plates. (b) Schematic of the relevant orientations in the original austenite matrix and final martensite lattices.

In figure 2 an atomic resolution view of the crossings at the $\alpha < 90°$ interface in figure 1a is presented. The tetragonality of the martensite lattice can directly be recognised by the rectangular dot patterns inside each variant on either side of the macrotwin. The longest edge of this rectangle corresponds with the elongating direction. Comparing the lattice images on both sides of the macrotwin it is seen that the broadest microtwin variant in both cases belongs to the same deformation variant, e.g., U_1. At the same time it is noted that this direction of elongation is parallel with the macrotwin interface, when disregarding the small rigid body rotations accompanying the transformation. From the same image it is seen that the small microtwin regions on both sides also belong to the same variant, e.g., U_2, as expected from the 90° angle between the two families of microtwin planes. These small variants penetrate into the opposite plate and taper and stop at a perpendicular small variant. Moreover, the tapered region is slightly bent towards the macrotwin interface. This tapering and bending occurs over a transition region of 5 – 10 nm across the interface. Alternatively, images of crossings at an interface with $\alpha > 90°$ reveal the direction of elongation of the broad variants perpendicular to the macrotwin. The bending of the fine tapered microtwins is in this case away from the macrotwin. All macrotwin interfaces consisting of crossings are found between martensite plates with very similar and constant volume fractions.

In order to get a more quantitative understanding on the central region around the macrotwin interface, power spectra of small areas of well defined high resolution patterns where performed. These are included in figure 2 and it can be concluded that the lattice deformations, i.e., numerical values for η_1 and η_3, in the transition region are equal, within experimental limits, to those in the plates, but the orientation of the lattice is halfway the two situations on either side. Apparently both plates cannot perfectly fit to one another without an extra accommodating rotation in between. The need for extra features accommodating remaining stresses is also confirmed by the occasional observation of dislocations at the macrotwin interface and a limited bending of the microtwins, up to 50 nm away from the interface and assisted by atomic ledges.

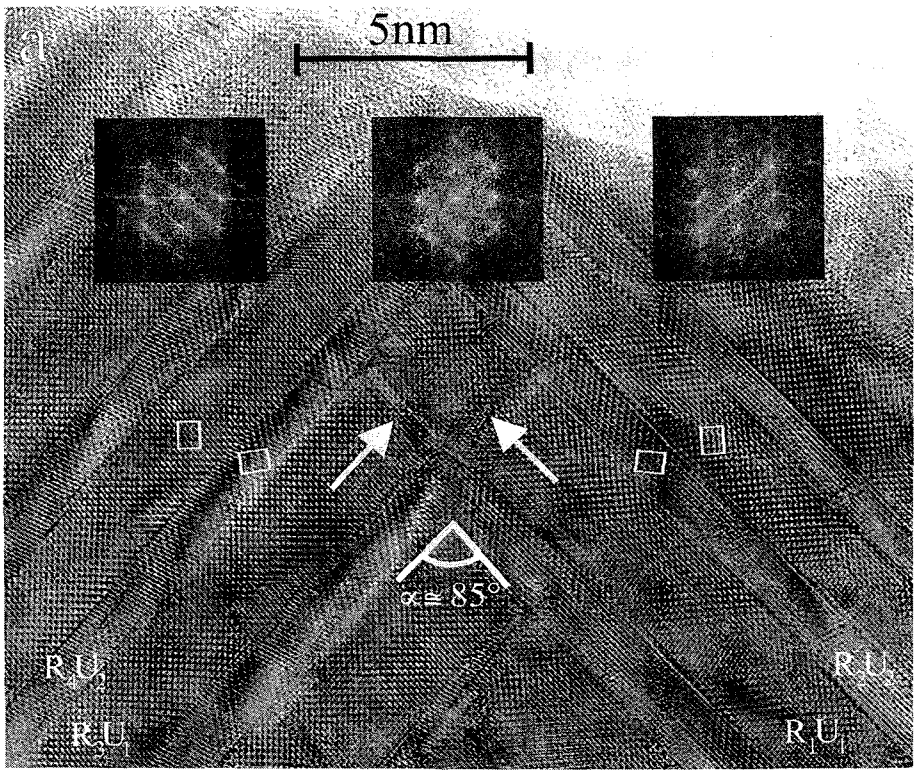

Figure 2: HRTEM image revealing the lattice configurations close to a $\alpha < 90°$ interface with crossing microtwins. The local deformations and orientations can be obtained from the included power spectra.

In figure 3 a high resolution image of a step configuration is shown. The transition layer that will allow the microtwin sequence to form a coherent interface with the pure variant is now restricted to the plate on the right while the other plate stays almost unaffected. The local deformation imposed is thus twice as large as the one requested for each plate in the crossing type boundaries. Again the broadest (finest) variants on both sides belong to the same deformation variant U_1 (U_2).

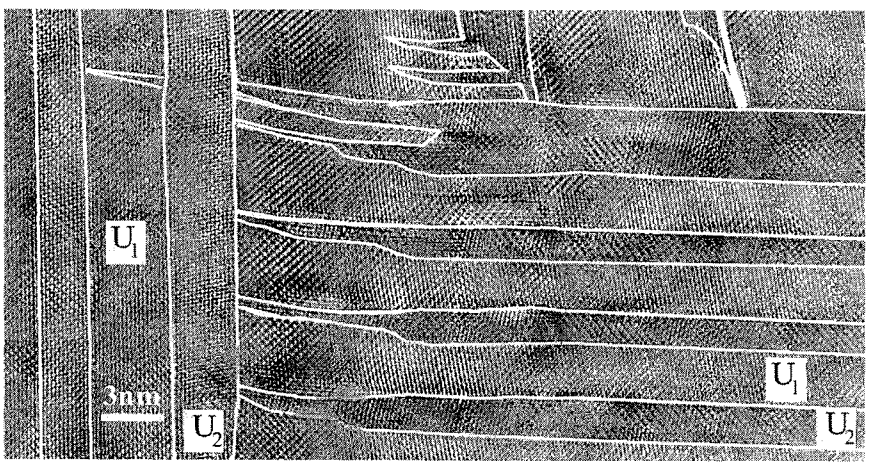

Figure 3: HRTEM image of a typical step configuration at a macrotwin boundary. The smaller variants of the right plate are seen to taper, bend and occasionally split when approaching the straight edge of a small variant of the left plate.

The transition from the core of the plate on the right part of the figure to the single variant U_2 on the left starts by a bending deformation which affects both U_1 and U_2 variants without apparent change of the volume fraction λ. The deformation is not a pure bending but is assisted by the appearance of dislocations. Getting closer to the interface, the thinnest variant (U_2) will disappear to the benefit of the other one (U_1) through the formation of a needle structure. The disappearance of the thin variant associated with the bending deformation leads to the formation of a twin configuration between variant U_2 of one laminate and variant U_1 of the other one. Only very small lattice distortions in the U_2 variant of the left plate are observed at the sites of the incoming needles. As can be seen from the top part of figure 3, the step configuration occurs in regions where the volume fraction differs strongly on both sides of the interface.

3. DISCUSSIONS

In the cubic-to-tetragonal transformation in Ni-Al, different martensite plates consisting of a sequence of two different variants of the product phase can nucleate and grow in the austenite matrix, as shown schematically in figure 4, in which the austenite is viewed along the $[001]_{B2}$ direction and the martensite along $<110]_{L10}$ directions, depending on the actual variant.

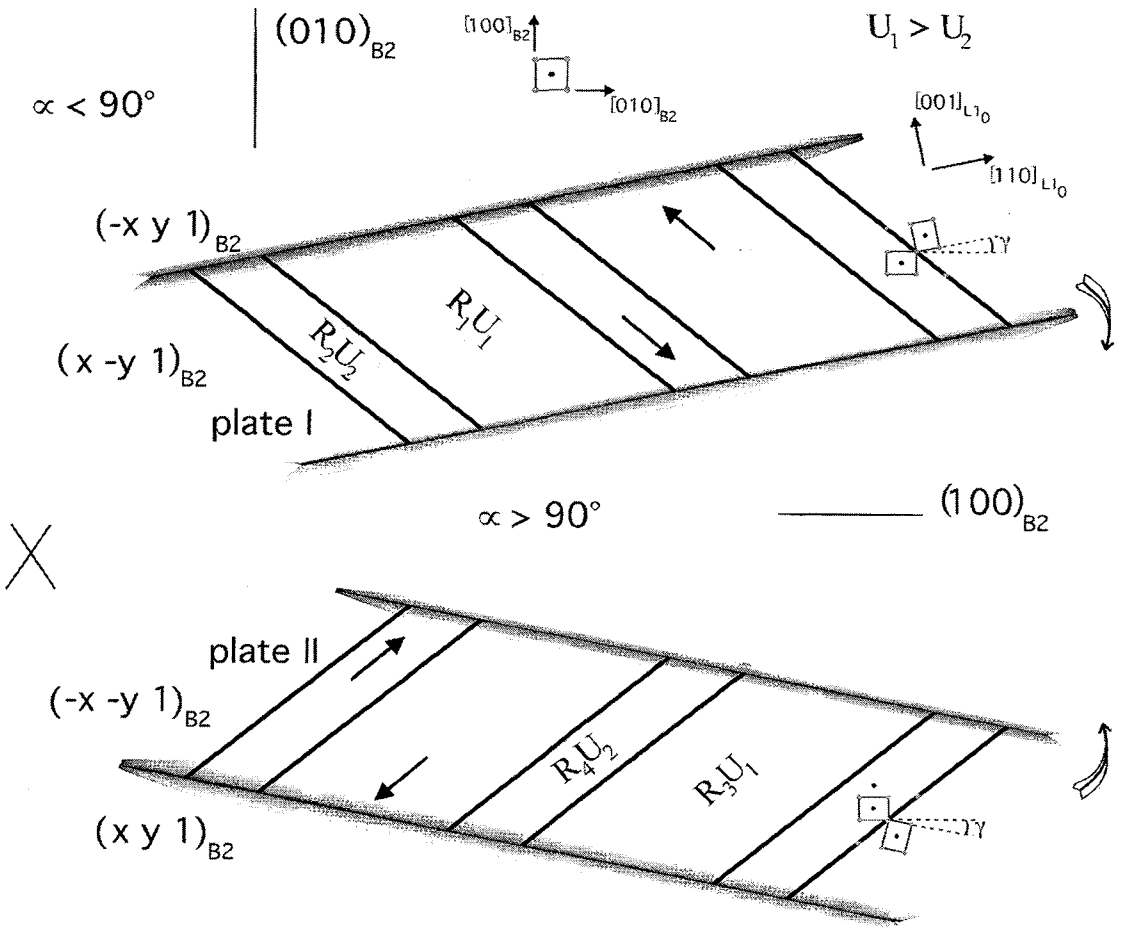

Figure 4: Schematic representation of the relative orientations of different features of two martensite plates that will finally make contact along cubic B2 planes.

The above described microtwins originate from prior $\{110\}_{B2}$ planes of the austenite. As the final microtwin configuration depends on the deformation parameters, some measures such as the angle γ and the volume fraction λ can be calculated in terms of the deformation parameters:

$$\cos\gamma = \frac{2\eta_1\eta_3}{\eta_1^2+\eta_3^2} \quad \text{and} \quad \lambda = \frac{1}{2}\left(1-\sqrt{1+\frac{2(\eta_1^2-1)(\eta_3^2-1)(\eta_1^2+\eta_3^2)}{(\eta_3^2-\eta_1^2)^2}}\right)$$

The angle γ corresponds with the total angle that has to be compensated by rotating the two variants involved within a given plate in order to close the gap between the deformed tetragonal lattices. As a start, both variants can be considered to rotate over the same but opposite angles $\pm\gamma/2$ around the normal to the plane of the drawing, thus yielding microtwin planes perfectly parallel with the prior austenite {110} planes. Any possible further rigid body rotation of the entire plate will of course destroy this balance so that the final orientation of one variant will be closer to its non-rotated tetragonal orientation than for the other. Because of the same mechanism the microtwin planes will no longer be parallel with the prior austenite {110} planes. Alternatively, one could assume that the absolute amount of rotation for both variants is different (i.e., one larger and one smaller than $\gamma/2$) again yielding microtwin planes deviating from the prior $\{110\}_{B2}$ planes.

For plate I in figure 4 the microtwin planes were chosen to originate from $(110)_{B2}$ planes and deformation variants U_1 and U_2 are combined, with U_1 occupying the largest volume. These choices fix the exact orientation of the microtwin planes and limit the possibilities for the habit plane to two. In the drawing, the microtwin planes are observed edge-on while the habit planes are inclined. Alternatively, plate II uses the same deformation variants with the same volume ratio (i.e., again volume U_1 > volume U_2), but a different set of microtwin planes, here $(1\text{-}10)_{B2}$, perpendicular to the previous family. Therefore crystallographically equivalent, but intrinsically different, habit planes will occur. Suppose now both plates nucleate separately in a given austenite grain, then they can join up in different ways. As the habit planes are distinctly different from any symmetry plane of the austenite, they can join along the austenite $(100)_{B2}$ or $(010)_{B2}$ planes and form different configurations. Indeed, joining along the $(100)_{B2}$ plane implies that the elongation directions (i.e., fct c-axis) of variants U_1 on either side are close to perpendicular to this new interface, which will become the macrotwin interface. On the other hand, joining along the $(010)_{B2}$ plane means that these directions are close to parallel with the formed macrotwin. These are exactly the features that are recognised from the HRTEM images and are thus indeed helpful in characterising the macrotwin interfaces.

At this point the small rotations of the microtwin planes with respect to their original $\{110\}_{B2}$ planes can be incorporated. The net angle of rotation θ can be calculated to be given by

$$\cos\theta = \frac{1+\eta_3 z^2}{(1+\eta_3)z} \text{ with } \quad z = \sqrt{\frac{\eta_1^{-2}+\eta_3^{-2}}{2}}$$

with the rotation axis being parallel with $(-\kappa\chi,\ \chi,\ \kappa\delta)$ where $\kappa = \pm 1$ defines the choice of the original cubic plane for the microtwin (+1 = plate I, -1 = plate II) and $\chi = \pm 1$ yields the two possible habit planes for each plate. δ is a constant obtained from the deformation parameters

$$\delta = \sqrt{\frac{\eta_3^2+\eta_1^2-2}{1-\eta_1^2}}$$

From the change in sign of the c-component it is clear that a change from (110) to (1-10) of the microtwin planes implies a rotation in opposite sense. Filling in typical values for the present austenite-martensite transformation it is found that a (110) family of microtwin planes with $U_1 > U_2$ (i.e., plate I) yields a clockwise rotation whereas a (1-10) family with the same choice of variant ratio undergoes a counter-clockwise rotation: these rotations are indicated in figure 4 as winged arrows.

In the same schematic the relative shearing directions in the different variants are also indicated. Assume the transformation fronts proceed outward from the nucleation point at X then the close packed planes of variant U_1 in plate I will shear in the upward direction while those of variant U_2 will shear downward, while the reverse is true for plate II. Opposite directions hold for the left parts of each plate, i.e., those extending to the left of the nucleation point at X. In order not to introduce too much strain, i.e., to compensate for these net shearings, the plates will rotate in the opposite directions, i.e., again in the directions of the winged arrows. This intuitive reasoning thus perfectly fits with the rigorous calculation of the angle θ. The difference in bending of the small variant tips can also be explained by referring to the shear directions. As for the $\alpha < 90°$ case the shearing of the U_1 variants is towards the interface it can be understood that this shearing also

pushes the fine needles towards this interface as both transformation fronts cross. On the other hand, for the $\alpha > 90°$ case, the U_1 shearing is directed away from the interface thus pulling the needles in the same direction. Both cases perfectly match the observations of figure 2 and similar images for the $\alpha > 90°$ case [5].

In order to evaluate the applicability of the continuum theories to the present problem, the measured and calculated angles should be compared. Precise numerical results, however, are hard to obtain as only the martensite lattice is observed in most of the present samples. As a result, the deformation parameters η_1 and η_3 can only be obtained from martensite images such as figures 2 and 3 by assuming volume preservation, which is a typical characteristic of shape memory material and is indeed the case to within 1% for the present material. Under this assumption, $\eta_1 = 0.93$ and $\eta_3 = 1.15$. The validity of this assumption can be checked by comparing the calculated values for the angle γ and the volume fraction λ measured away from the macrotwin interface. In Table I a comparison between these and other measured and calculated parameters is presented.

Table I: theoretical and experimental microstructural parameters based on deformation parameters $\eta_1 = 0.93$ and $\eta_3 = 1.15$ measured in the assumption of volume preservation

	γ	λ	θ	α
theory	12.1°	0.35	2.9°	93.7°, 86.3°
experiment	12.5°	0.35	-	95°, 85°

Comparing the calculated and observed values for γ and λ indicates that the assumption of volume preservation is indeed valid. In order to avoid the effects of local deformations near the macrotwin interface, the experimental values for α should be measured between the microtwin orientations far away from the macrotwin interface. As the axis of the rigid body rotation is not exactly along the $[001]_{B2}$ direction, a correction using trace analysis is necessary, yielding the final values for α. From these numbers it is concluded that the tendencies as well as the order of magnitudes are properly described by the theory in the assumption of separately ucleating plates. Still, local differences lead to severe deviations in the measured parameters.

One possible explanation for this discrepancy could be, as was shown by Bhattacharya, the fact that a $\{100\}_{B2}$ macrotwin interface between two microtwinned plates with close to perpendicular families of microtwin planes, cannot exist as a zero-energy configuration for the cubic-to-tetragonal transformation [6]. This also implies that the observed 90° configurations are expected to show structural features which accommodate the remaining stresses occurring when both plates actually meet. As indicated above, local reorientations of the lattice in the transition region of the crossing type as well as occasional dislocations indeed occur at the macrotwin interfaces. Moreover, some curvature of the microtwins, accommodated by atomic step ledges, was observed further away from the macrotwin.

Also the step type parts of the interface reveal severe local lattice deformations. In an attempt to quantify these deformations the change in orientation of the close packed planes of the right plate in figure 3 when approaching the macrotwin interface was measured. Assuming small stresses, it can be shown that in the framework of two-dimensional linear elasticity the angle ε is a function of the changing volume fraction $\lambda(x)$ with the deformation parameters η_1 and η_3 and the volume fraction λ_∞ far away from the interface as numerical variables:

$$\sin\varepsilon(x) = 2\left(\frac{\eta_1}{\eta_3} - 1\right)(\lambda_\infty - \lambda(x))$$

In figure 5 a comparison between measured and calculated values for ε as a function of the distance x from the step interface is given, from which a good qualitative agreement between the experimental data and suggested theoretical behaviour is found.

The only structural difference that could be detected from the still images of the final situations is the appearance of strong differences in local variant widths at the site of the steps. The atomic detail described above indicates that in these less symmetric cases the system takes advantage of the fact that large contact regions between two variants of the same deformation type can be avoided, which is indeed prohibited for zero-energy configurations in the schemes of the elastic theories[7]. In a more general way, this difference could possibly reflect a competition between the elastic and surface energy contributions [8]. In order to do so, needles of the smallest variant are formed in one plate, ending at a flat edge of the same variant in the other plate. The choice for needle formation of the smallest variant is understandable as this implies less bending of the microtwin planes involved. This immediately dictates the type of variant that will form the actual interface as being of the same type. This way the primary contact regions are between U_1 of the needle

forming plate and U_2 of the other plate, a contact that according to theory can indeed provide energy minimisation[7]. For the latter, however, well-defined orientation relations should appear which can indeed exist within a given plate but are violated by some degrees when dealing with variants belonging to different plates. In order to compensate for this disadvantage the system includes an extra deformation in the plate containing the needles.

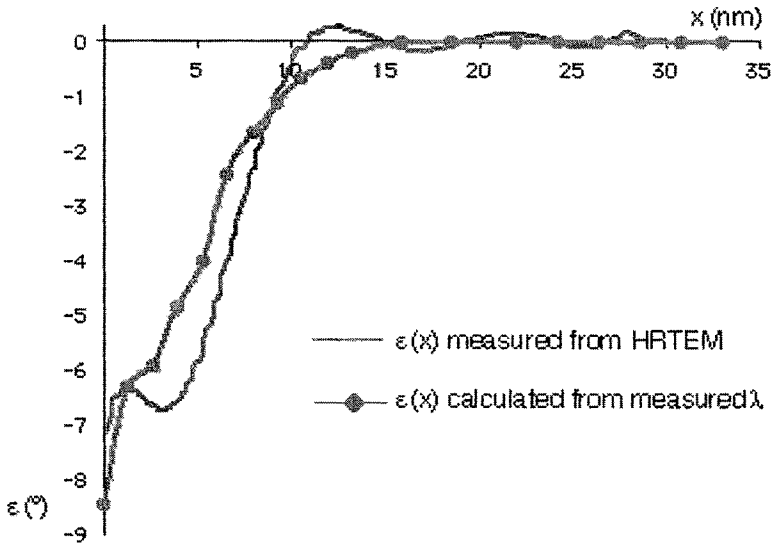

Figure 5: Comparison between calculated and measured change in orientation of variant U_1 of the right plate in figure 3 as a function of the distance from the interface.

Overall, when comparing materials prepared by different techniques, interfaces in splat-cooled material seem to accommodate more steps while in bulk material the preference is on crossings, which can be related to the general observation that the fixed volume fraction and thus the microtwin variant widths are less stable in splat-cooled material [9]. Recent TEM results on melt-spun material also reveal a large number of step configurations at the macrotwin interfaces [10].

Remains the question why only configurations with the same deformation variant for the widest twin bands are observed. Again, no definite answer to this question could be found from the final still images. Still, as the actual environment of a single grain or a set of growing martensite plates within a grain is most probably not perfectly isotropic, it could be argued that each austenite grain or each group of plates will (trans)form with a preferential direction for elongation. This would then single out one martensite variant to have a larger fraction within a given region of the sample. As such a region contains numerous macrotwins, the chance of observing one with equal deformation variants for the widest twins on both sides is much higher than the chance of finding the one case at the interface of two such grains or subregions.

4. CONCLUSIONS

In the present work atomic scale details of martensite plate interfaces, so-called macrotwin boundaries, formed by two coalescing microtwinned martensite plates in Ni-Al are described and discussed. Only configurations with two families of microtwin planes at angles close to 90° are retained. Depending on the original orientation of the separate plates the angle between the microtwin planes on either side of the macrotwin interface can be larger or smaller than 90° by about 5°. These relative angles correspond well with calculations based on energy minimisation of the original orientations of the respective martensite plates involved.

Irrespective of this angle, two structural configurations are found differing in local micro- and atomic structure. For the crossing type, a transition region of approximately 5 – 10 nm between both coalesced plates is observed in which the different rigid body rotations of both plates are compensated in a quasi-continuous manner. Small microtwin variants from one plate form bending needles tapering towards the

perpendicular microtwin interfaces in the other plate, thus producing the crossed view of this type. This case occurs when the microtwin volume fractions on both sides of the macrotwin interface are similar. In the step type, occurring when measurable differences between the microtwin volume fractions on both sides are observed, only one plate forms bending needles, which usually do not penetrate into the next plate.

While the described macrotwin configurations hold for both bulk and splat-cooled materials, the only difference which could be made between these materials is the relative amount of step type versus crossing type configurations. Even if a statistical analysis based on HRTEM results is hazardous, the step type configurations appear to be more commonly observed in splat-cooled material. In our opinion, this feature is only related to the fact that noticeable changes in the width of the deformation variants are more often observed in splat-cooled than in bulk material as illustrated in a previous work.

Acknowledgements

The authors like to thank K. Bhattacharya, R. James, S. Conti and S. Müller for stimulating discussions and D. Holland-Moritz for the preparation of the splat-cooled samples. This work was supported by the Trade and Mobility Research program of the EEC under the project FMRX-CT98-0229 (DG12-BDN) and within the IUAP network entitled "Phase Transitions in Crystalline Solids".

References

1. S. Chakravorty and C.M. Wayman, Metall. Trans. A **7**, 555 (1976).
2. S. Chakravorty and C.M. Wayman, Metall. Trans. A **7**, 569 (1976).
3. I. Baele, G. Van Tendeloo and S. Amelinckx, Acta metall. **35**, 401 (1987).
4. D. Schryvers, Phil. Mag. A. **68**, 1017 (1993).
5. P. Boullay, D. Schryvers and J. Ball, Acta materialia (to be published).
6. K. Bhattacharya, Acta metall. mater. **39**, 2431 (1991).
7. J.M. Ball and R.D. James, Arch. Rat. Mech. Anal. **100**, 13 (1987).
8. S. Conti, private communication .
9. D. Schryvers and D. Holland-Moritz, Intermetallics **5**, 427 (1998).
10. P.L. Potapov, P. Ochin, J. Pons and D. Schryvers, Acta materialia (submitted for publication).